

Lambda-ABF-OPES: Faster Convergence with High Accuracy in Alchemical Free Energy Calculations

Narjes Ansari,^{*,†} Francis Jing,[†] Antoine Gagelin,[†] Florent Hédin,[†] Félix Aviat,[†]
Jérôme Hénin,[‡] Jean-Philip Piquemal,^{†,¶} and Louis Lagardère^{*,†,¶}

[†]*Qubit Pharmaceuticals, 29 rue du Faubourg Saint Jacques, 75014 Paris, France*

[‡]*Laboratoire de Biochimie Théorique, UPR 9080 CNRS, Université de Paris Cité, 75005
Paris, France*

[¶]*Laboratoire de Chimie Théorique, Sorbonne Université, UMR 7616 CNRS, 75005 Paris,
France*

E-mail: narjesa@qubit-pharmaceuticals.com; louis.lagardere@sorbonne-universite.fr

Abstract

Predicting the binding affinity between small molecules and target macromolecules while combining both speed and accuracy, is a cornerstone of modern computational drug discovery which is critical for accelerating therapeutic development. Despite recent progresses in molecular dynamics (MD) simulations, such as advanced polarizable force fields and enhanced-sampling techniques, estimating absolute binding free energies (ABFE) remains computationally challenging. To overcome these difficulties, we introduce a highly efficient, hybrid methodology that couples the Lambda-Adaptive Biasing Force (Lambda-ABF) scheme with On-the-fly Probability Enhanced Sampling (OPES). This approach achieves up to a nine-fold improvement in sampling efficiency and computational speed compared to the original Lambda-ABF when used in conjunction with the AMOEBA polarizable force field, yielding converged results at a fraction of the cost of standard techniques.

Introduction

Accurately predicting the binding affinity between a small molecule (ligand) and its target (protein or RNA/DNA) is a fundamental tool in modern computational drug discovery, that can be used both at the hit discovery and at the lead optimization stages.¹ Indeed, it minimizes the cost of such project by reducing the need to rely on experimental assays.

Recent advancements in molecular simulation, especially in molecular dynamics (MD), have greatly enhanced our ability to predict binding affinities. One of the most complex challenges in this area is the prediction of absolute binding free energies (ABFE),² which depend on two key factors: reliable force fields (FF) and efficient sampling.³⁻⁵ Force fields must accurately capture complex and subtle molecular interactions—such as electrostatics (ELE), van der Waals (VDW), and solvation effects—while also accounting for factors like protonation state variations and conformational flexibility. Efficient sampling is also essential to explore the vast configurational space of ligand-protein interactions and is often limited

by complex free energy barriers.

In this context, the development of high-quality polarizable force fields,^{6–8} such as AMOEBA,^{9–12} and tools like Poltype¹³ for accurately parametrizing complex ligands, have significantly enhanced the accuracy of MD simulations.^{14–19} These progresses allow for more accurate modeling of ligand-protein interactions and a more reliable prediction of associated thermodynamic properties, such as the binding affinity.¹⁹

Still, MD simulations encounter sampling limitations, especially in biological systems such as ligand-protein complexes. Indeed, the exploration of the conformational space is often hindered by significant free-energy barriers, associated to time scales beyond the reach of unbiased MD simulations, making it challenging to sample all relevant states exhaustively in standard simulations.

To address these challenges, several enhanced sampling algorithms have been developed. Notably, Collective Variable (CV)-based importance-sampling techniques such as Umbrella Sampling (US),²⁰ Adaptive Biasing Force (ABF),^{21–23} MetaDynamics (MtD),^{24,25} its recent evolution, On-the-fly Probability Enhanced Sampling (OPES),^{26,27} and Temperature-Accelerated Molecular Dynamics (TAMD)²⁸ have demonstrated significant success. These algorithms rely on the definition of CVs, reduced dimensions along which biasing forces, potentials, or probabilities are applied to facilitate sampling of the system’s configuration space. Each enhanced-sampling method has its advantages and limitations.⁴ To overcome these challenges, hybrid methods have been developed to combine different techniques and mitigate their individual limitations.²⁹

Another class of methods, called alchemical approaches, estimates free energy differences associated to unphysical “alchemical” changes of the molecular Hamiltonian³⁰ by scaling some key interactions with an alchemical parameter $\lambda \in [0, 1]$. They have proven useful to compute solvation as well as binding free energies. Traditional techniques involve several simulations at fixed λ values and the reconstruction of the free energy difference of interest through an estimator such as the Free Energy Perturbation (FEP)³¹ or the Thermodynamic

Integration (TI)³² one.

Alternatively, another approach called lambda-dynamics³³ was introduced, in which the coupling parameter λ is treated as a dynamical variable through an extended Lagrangian/Hamiltonian scheme. Building upon this concept, we introduced a new alchemical method, Lambda-Adaptive Biasing Force (Lambda-ABF),³⁴ that leverages lambda dynamics in combination with multiple-walker ABF,³⁵ enabling efficient sampling of λ as a collective variable (CV). It has been shown to be robust and to improve sampling efficiency compared to standard fixed-lambda methods.³⁴ Additionally, in the context of binding simulations, it leverages Distance-to-Bound-Configuration (DBC)³⁶ restraints to keep the ligand within the binding pocket, limiting its translational, rotational, and conformational fluctuations. Compared to fixed-lambda methods, Lambda-ABF not only reduces the computational cost but is also arguably simpler as it bypasses the definition of a λ schedule and portable thanks to its implementation within the Colvars library.^{37,38}

ABF applies biasing forces along the transition coordinate to flatten the sampled free-energy landscape toward a uniform distribution. It is well understood mathematically²³ and is associated to a local (unconstrained) TI free-energy estimator. A key limitation arises with barriers along other degrees of freedom which can lead to kinetic trapping in some regions and overall non-ergodic sampling and also in the diffusive regime when (local) convergence is reached.

To overcome this limitation, we combine Lambda-ABF with the exploratory version of the OPES method, known as OPES-Explore.²⁷ Hereafter, we will simply refer to it as OPES. This method is CV-based and aims at sampling a target probability distribution associated to lower barriers. It can be seen as an evolution of (well-tempered) MetaDynamics with an emphasis on exploration and is user-friendly as it requires only a few physically motivated parameters to be set. By applying a bias to the lambda CV within the Lambda-ABF-OPES method, we effectively integrate the strengths of both ABF and OPES.

Similarly to the (wt)meta-eABF method,²⁹ the Lambda-ABF-OPES approach benefits

from the combination of ABF and OPES. While ABF reduces the free energy barriers, OPES fills the energy valleys by incorporating a history-dependent potential term. To our knowledge, this is the first instance of combining ABF with the OPES method in an alchemical framework. This approach improves convergence speed, enhancing it by up to 9 times compared to the original Lambda-ABF method.

We applied this hybrid approach, utilizing the AMOEBA polarizable force field and DBC restraints, to calculate the absolute binding free energy of 11 diverse small drug-like molecule inhibitors binding to bromodomains (BRD4), a well-studied macromolecular system.^{39–42} Our results show that while maintaining high accuracy, with a mean absolute error of 0.90 kcal/mol, we achieved a significant improvement in convergence speed. This represents a notable advancement, particularly when using the more computationally demanding AMOEBA polarizable force field.

The close agreement between our computational predictions and experimental data demonstrates the robustness of our hybrid method, offering a promising approach for computational drug design.

Methods

MD Simulations

We performed all simulations using the molecular dynamics code Tinker-HP Version 1.2,^{43,44} which includes the Colvars library³⁷ for Lambda-ABF-OPES simulations. For the protein, water, and ion parameters, the polarizable AMOEBA force field^{9–12} was applied. Ligand parameterization was performed using the Poltype package.¹³ The systems, containing between $\sim 31,000$ and $\sim 42,000$ atoms on average (varying with ligand size), were neutralized with 0.15 M physiological NaCl concentration. A cubic water box with dimensions of 70–80 Å was used, ensuring a minimum distance of 12 Å between the ligand and the box edge, with its size adjusted according to the ligand.

The systems were first minimized using the Tinker-HP `minimize` program, followed by a two-step heating process from 200 K to 298 K under the NVT ensemble. In the first step, restraints were applied to all protein-ligand and X-ray water molecule atoms. In the second step, restraints were applied to heavy backbone atoms, using a force constant of 10 kcal/mol/Å² in both steps. Each stage included 4 ns of MD simulations, conducted using the RESPA integrator with a time step of 2.0 fs.

In the third step, the three-level multiple timestep BAOAB-RESPA1 integrator⁴⁵ with an outer timestep of 10 fs (and an intermediate of 3.33 fs and a shorter timestep of 1 fs) was employed under the NVT ensemble for 5 ns, with restraints applied only to C α atoms using a force constant of 1 kcal/mol/Å². This was followed by equilibration in the NPT ensemble at 1 atm for 5 ns, maintaining the same restraints as the previous step. Finally, for each ligand, a production run of at least 100 ns was performed under the NPT ensemble using the BAOAB-RESPA1 Langevin integrator with a 10 fs time step. During the production phase, a restraint with a force constant of 1 kcal/mol/Å² was applied to the C α atoms of the protein’s floppy tail to prevent large conformational changes.

Non-Langevin temperature control was ensured by using the Bussi thermostat⁴⁶ and pressure with the Berendsen barostat.⁴⁷ Van der Waals interactions employed a 12 Å cutoff, while electrostatic interactions were treated using the Particle Mesh Ewald (PME) method⁴⁸ with a real-space cutoff of 7 Å. Induced dipoles were calculated with a Preconditioned Conjugate Gradient (PCG) solver, with a convergence tolerance of 1×10^{-5} Debye.⁴⁹

DBC Restraint

In alchemical methods, absolute binding free energy calculations critically depend on a precise definition of the bound state and well-designed ligand restraints (both translational and, optionally, orientational) to ensure rapid convergence. In this study, we employed the DBC coordinate to restrain the ligand during Lambda-ABF-OPES simulations. It is defined as the RMSD of some ligand atoms (LA) for each frame, with the alignment performed rela-

tive to some atoms of the receptor’s binding (RB) site.³⁶ This approach captures positional, orientational, and also conformational deviations of the ligand in a single collective variable.

To select the LA, we monitored the root mean square fluctuation (RMSF) of the ligand’s heavy atoms over at least 100 ns of standard MD simulations. Atoms with an RMSF of less than 0.6 Å were selected for tight binders (Ligands 1-9), while those with an RMSF between 0.7 and 0.8 Å were chosen for weak binders (Ligands 10-11). For the RB selection, we used the C α atoms of the protein within 6 Å of the ligand, with an RMSF of approximately 0.6 Å. See Fig. S1 in the SI for the definition of DBC for the protein and each ligand. During plain MD of each ligand, the DBC was monitored using the Colvars library, and the DBC value within the 95% interval of the distribution was selected as the DBC cutoff for the restraint in Lambda-ABF-OPES. This selection ensures that during the alchemical simulation, there is no biased artifact from the DBC restraint. The DBC cutoff for each ligand is listed in Table S3 SI. A flat-bottomed harmonic restraint was then applied to the DBC with a force constant of 100 kcal/mol/Å² above the DBC cutoff.

Lambda-ABF-OPES for Calculation of Absolute Binding Free Energies

Details of the Lambda-ABF and OPES-Explore methods can be found in the original publications.^{26,27,34} Here we provide a brief overview of their underlying theories.

The Lambda-ABF algorithm^{21,22,34} adaptively computes the derivative of the free energy associated with the parameter λ using the thermodynamic integration (TI) formula.⁵⁰ This estimate is applied as a force directly to the simulated system, guiding the dynamics. As a result, the sampling of λ converges toward a uniform distribution, facilitating the crossing of free-energy barriers.

OPES-Explore,²⁷ a collective-variable (CV)-based enhanced sampling technique, represents the latest advancement in the MetaDynamics family. It broadens the sampling of a system toward a target probability distribution, known as the well-tempered distribution.

This approach employs Gaussian kernels to adaptively construct a bias potential, guiding the system’s exploration while preserving thermodynamic relevance. Critical parameters, such as the Gaussian kernel width and bias factor, are pivotal in defining the sampling’s scope and stability. Additionally, the barrier parameter (ΔE) ensures efficient transitions between basins while preventing access to irrelevant high-energy states.

In this study, the ABFE is calculated by continuously “alchemically” decoupling the ligand from its environment, both in complex with the protein and separately in bulk solvent. The standard free energy of binding is then determined using a thermodynamic cycle,⁵¹ which requires sampling of the alchemical Hamiltonians. We employed the Lambda-ABF approach as implemented in Tinker-HP/Colvars, in combination with OPES-Explore provided by the Colvars library³⁷ version 2024-11-18. This integration provides user-friendly convergence estimation without requiring post-processing and allows seamless compatibility with other CV-based methods.

All simulations were performed at $T = 300$ K and $P = 1$ Atm using the BAOAB-RESPA integrator⁴⁵ with a 3 fs time step under the NPT ensemble, employing four walkers⁵² to separately decouple the VDW and ELE interactions. More precisely, the polarizabilities and permanent multipoles of the ligand are scaled down to 0 in the electrostatic legs (ELE), and the van der Waals interactions between the atoms of the ligand and all the other ones are scaled down to 0 (leveraging softcore interactions⁵³) in the van der Waals legs (VDW). In the complex phase, 30 ns were simulated for the VDW leg and 5 ns for the ELE leg. In the solvent phase, both the VDW and ELE legs were simulated for 5 ns each.

As mentioned earlier, for OPES-Explore, the barrier parameter is a critical setting in the simulations and must be sufficient to ensure that the method accurately captures the energy landscape and transition state barriers. We conducted tests using OPES-Explore alone with different barriers. The final ΔG values varied between runs (see SI), indicating that OPES-Explore alone struggles to compute the binding free energies of interest. However, when combining OPES-Explore with Lambda-ABF, the system is primarily driven by Lambda-

ABF, which facilitates the crossing of energy barriers, and also benefits from the rapid convergence of the TI estimator. In this case, OPES-Explore mainly serves to push the system out of local minima. Therefore, the barrier parameter does not need to be equal to the free energy differences associated to the simulation. Our tests showed that setting the bias threshold of OPES-Explore to a minimum of 5 kcal/mol for both the ELE and VDW legs in the complex and solvent phases effectively accelerated the convergence across all ligands, regardless of their respective energy barriers. For ligand 11, a threshold of 2 kcal/mol was sufficient for proper acceleration. Although a barrier of 5 kcal/mol also works well, since this ligand is a weak binder, the lower threshold of 2 kcal/mol ensures better stability in convergence. An adaptive sigma is used to determine the Gaussian kernel width, and the frequency for kernel deposition was set to 300 steps, which corresponds to 9 ps with a time step of 3 fs.

For Ligand 11, during the 180 ns plain MD simulations, we observed two equally plausible binding modes in which the trifluorotoluene moiety was flipped by 90° , consistent with the result of Ref. 41. Consequently, ABFE calculation was performed for each binding mode, resulting in a total of two binding free energy calculations. The results from multiple binding modes were combined into a single binding free energy value as described in Ref. 54.

The free energy cost associated with the release of the DBC restraint is computed in the gas phase through TI by progressively releasing it to a compatible harmonic distance restraint which can then be computed analytically.^{34,36,51}

In these simulations, we observed that the rotamers of Asn140 in the Apo state may adopt a conformation favorable in the Apo state but not in the Holo state (see Results and Discussion and SI for more details). This could lead to sampling the Holo state with an incorrect orientation of Asn140, potentially introducing artifacts. The restriction (through a restraint) to one of these rotamers as an Apo endpoint must be accounted for. Therefore, a positional restraint was applied to the heavy atoms of the Asn140 residue and its neighboring atoms (all heavy atoms of the backbone and those within 6 Å of the ligand with a mild

force constant of 2 kcal/mol/Å²). This restraint was necessary to ensure that Asn140 and its neighboring atoms were properly sampled in both the Apo and Holo states, given the continuous switching of lambda between 0 (Apo) and 1 (Holo) in the Lambda-ABF-OPES simulations. Since both rotamers of Asn140 are equally favorable in the Apo state (see Fig. 2), an RTln(2) correction was added to the final computed ΔG . In addition, to avoid artifacts during alchemical decoupling as described in SI, the C α atoms of BRD4 were restrained to their relaxed configuration.

Analytical Lambda Derivatives for Variational Many-Body Potentials

As all TI-based technique, Lambda-ABF requires the computation of potential derivatives with respect to the alchemical parameter λ which are not trivial to compute for many-body interactions such as polarization as present in the AMOEBA force field. In our previous work³⁴ we used a simple interpolation of polarization between the end states which gives immediately the associated derivatives as the difference of these, but this is associated with an increase of the computational cost because of the need to solve 2 polarization equations at each timestep. Recently, analytical derivatives associated to a simple scaling of the polarizabilities and multipoles have been introduced.⁵⁵ Here we resorted to a more general formulation relying on the variational formulation of the many-body term and the Hellman-Feynman theorem: $E_{pol}(\mathbf{r}, \lambda) = E_{pol}(\mathbf{r}, \lambda, \boldsymbol{\mu}(\mathbf{r}, \lambda))$ and

$$\frac{dE_{pol}}{d\lambda} = \frac{\partial E_{pol}}{\partial \lambda} + \frac{\partial E_{pol}}{\partial \boldsymbol{\mu}} \frac{\partial \boldsymbol{\mu}}{\partial \lambda} = \frac{\partial E_{pol}}{\partial \lambda}$$

because of the minimum conditions on the induced dipoles. Note that this formulation still holds for other many-body terms with similar variational formulation as is the case for fluctuating charges,⁵⁶ continuum solvation models⁵⁷ or QM-MM.^{58,59} Further development of the gradients used in this work using Particle Mesh Ewald is given in Technical Appendix.

Results and Discussion

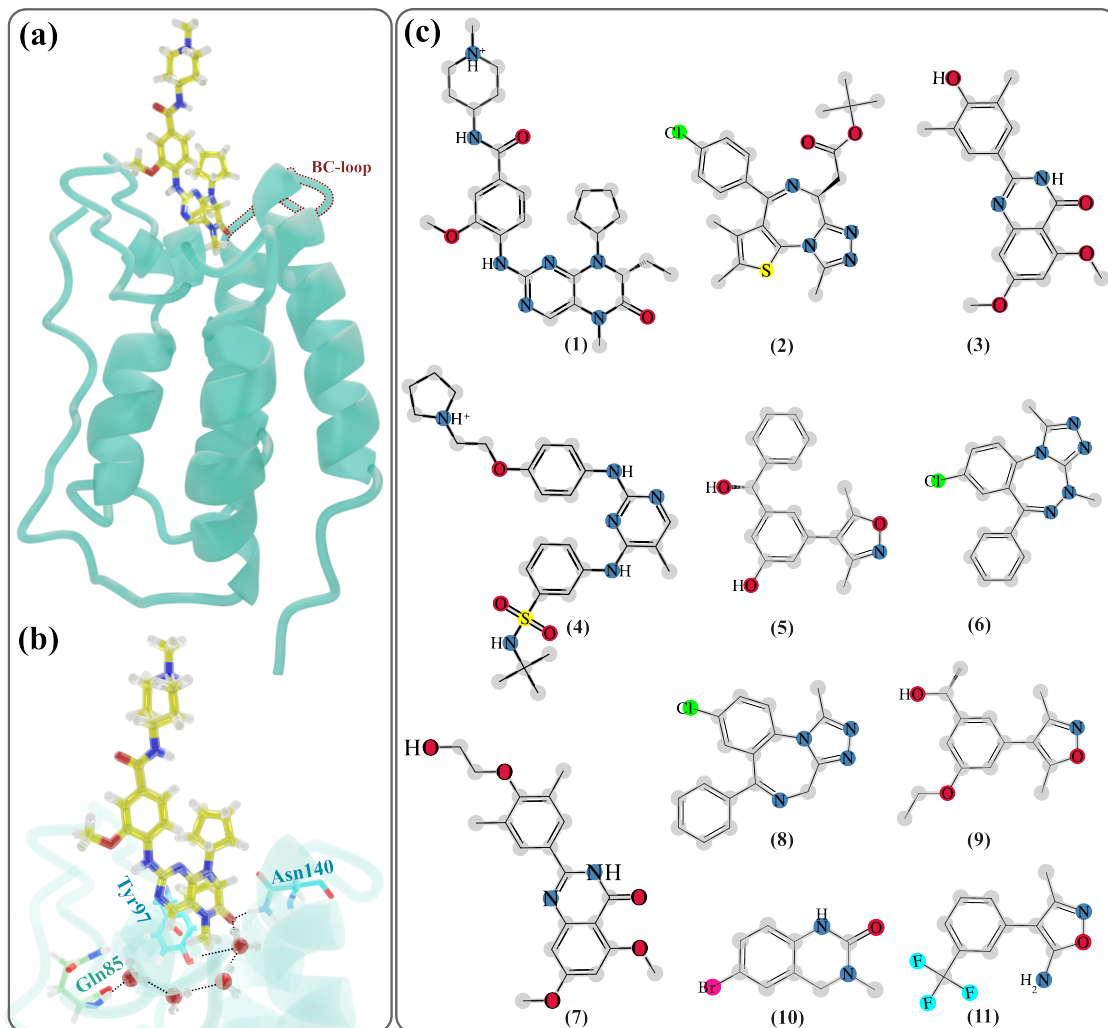


Figure 1: **Structural representation of the BRD4-ligand complex.** (a) Cartoon representation of the BRD4 bromodomain structure in complex with ligand 1 (PDB ID: 4OGJ), with the BC-loop highlighted using a dashed marker. (b) Binding mode of BRD4 with the ligand, highlighting key interacting residues Asn140 and Tyr97 in cyan. Crystallographically observed water molecules are shown as ball-and-stick representations, along with the hydrogen bond network bridging the ligand and protein via Tyr97 and Gln85 residues. The protein is represented as a transparent cartoon. (c) The 2D structures of the compounds analyzed in this study are shown and labeled with Arabic numerals in descending order of binding affinity.

In the following section, we will first provide a brief overview of the general binding modes of the 11 ligands in the BRD4 system. We will then focus on the orientation of the Asn140 residue, a key residue that directly interacts with the ligands, in both the Apo and Holo

states, highlighting any significant differences. Finally, we will examine the binding affinities and correlate these findings with the experimental values.

As depicted in Fig. 1(c), the 11 ligands are large, flexible, drug-like molecules, some of which are charged (Ligand 1 and 4). These characteristics make them an ideal set for evaluating the performance of the new method. All ligands target a common binding site. Asparagine (Asn140), located within the BC-loop binding pocket (Fig. 1(a)), is the most critical residue, which interacts directly with the ligands. The side chain of Asn140 consists of an amide group ($-\text{CONH}_2$) attached to a $\text{C}\beta$, which is itself connected to the $\text{C}\alpha$ of the backbone via rotatable bonds.

The 100 ns plain MD simulations for all ligands (except Ligand 11, for which 180 ns was run) show that, in the Holo state, only one rotamer is favorable due to the formation of salt bridges between the ligands and the Asn140 residue (Fig. 1(b)). However, in the Apo state, both rotamer states can be present. To investigate this, we calculated the free energy associated with the two rotamers in the Apo state using the OPES method (see SI for more details). Fig. 2 shows that the two rotamers are equally favorable and that switching between them can happen naturally.

In addition to Asn140, four conserved (polarizable) water molecules⁶⁰ in the binding site of BRD4 also play a crucial role in stabilizing the ligands within the binding pocket, thereby enhancing binding affinities. As illustrated in Fig. 1(a), one of these water molecules forms a bridge between the Tyr97 residue and the ligand (except for Ligand 4). To preserve this stabilization, the X-ray water molecules were retained in the binding pocket during system preparation, as they contribute to a hydrogen-bond network involving the three other conserved water molecules and the protein.

Using the equilibrated structures, we carried out absolute binding free energy calculations employing the novel Lambda-ABF-OPES method. The correlation plot between experimental values and calculated results is shown in Fig. 3 and reported in Table 1.

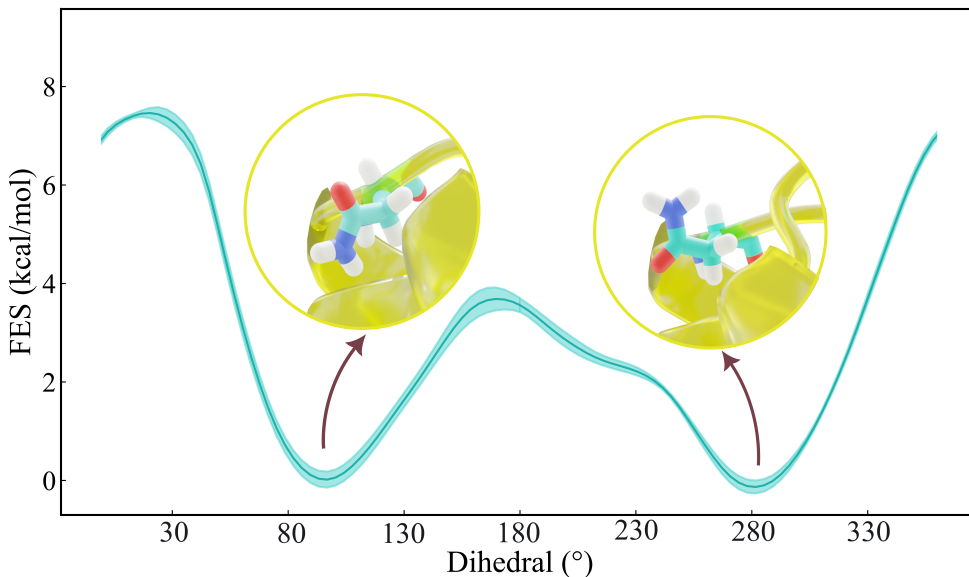


Figure 2: **Free energy surfaces (FES) of the χ_2 dihedral angle for the Asn140 residue** obtained from plain OPES simulations, starting the Apo structure (PDB ID: 4LYI). Two different rotamers of Asn140 corresponding to each minimum are represented. The protein is depicted in a cartoon representation in yellow, while Asn140 is shown as a stick representation. χ_2 is the torsion angle between the nitrogen and the carbonyl carbon of the amide group. The transparent regions indicate the associated errors of the FES, calculated over block analysis.

We observe a strong correlation between the experimental and calculated results, with a Pearson’s correlation coefficient (Pearson’s r) of 0.81. The analysis yielded a root mean square error (RMSE) of 1.1 kcal/mol and a mean absolute error (MAE) of 0.9 kcal/mol. These results are consistent with experimental data and align well with those reported in Refs. 40,41. The key advantage of this method lies in its user-friendliness, reduced computational resource requirements, and rapid convergence. Compared to Lambda-ABF, the traditional fixed Lambda approach,⁴¹ and the newly developed CV-based approach,⁴⁰ this method offers significantly improved computational efficiency while maintaining high accuracy. These attributes make it particularly well-suited for large-scale or high-throughput applications.

To evaluate the robustness of the method, we performed a detailed convergence test by analyzing the convergence time of ΔG and comparing the results with those obtained

using Lambda-ABF alone. The convergence time was defined as the point from which all subsequent data points remain within the specified tolerance of the mean, providing a clear metric for determining when the simulation data stabilizes. A tolerance of 0.2 kcal/mol was used in this analysis, representing just 20% of the commonly accepted convergence threshold for binding free energy calculations. This strict criterion underscores the precision and reliability of the method.

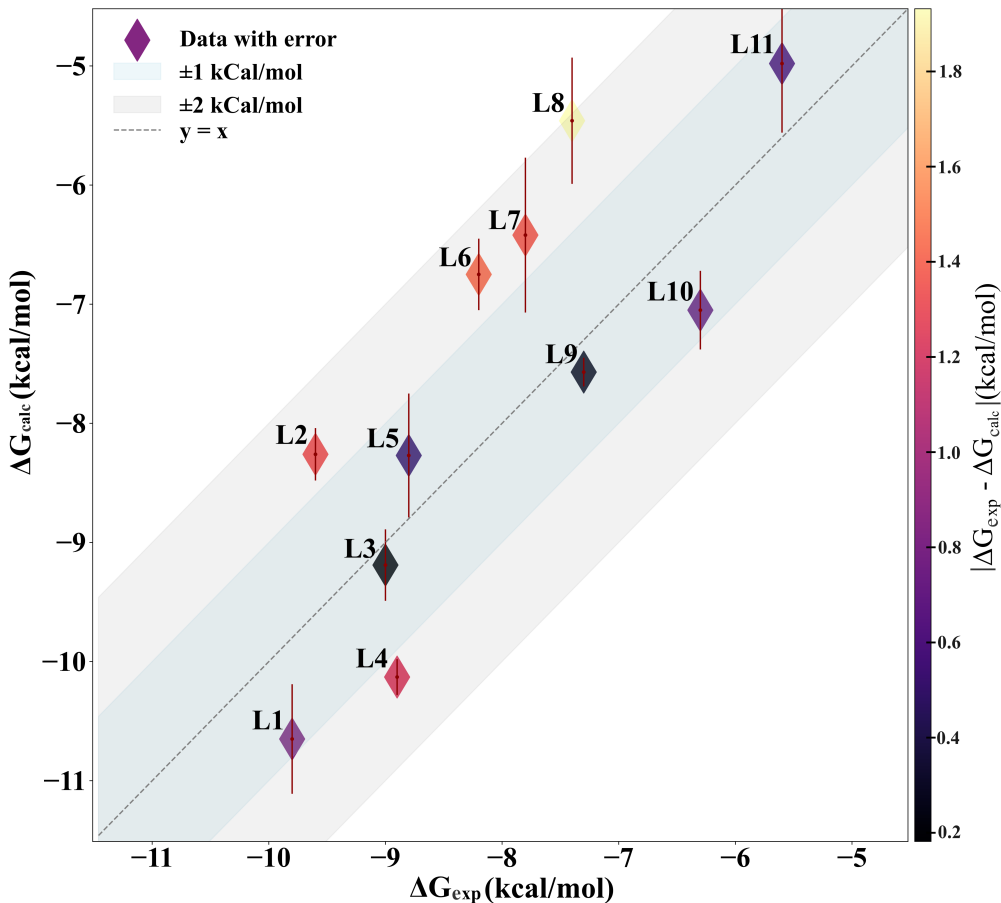


Figure 3: **Experimental vs Calculated ΔG values.** Calculated ΔG and errors are the mean and standard error from the mean from three repeats for each ligand. The dark shaded region spans ± 1 kcal/mol; the lighter region spans ± 2 kcal/mol. The color bar represents the absolute value difference between experimental and computed values. Pearson' r , RMSE, and MAE are 0.81, 1.10, 0.90 kcal/mol respectively.

Figure 4 illustrates an example of a ΔG convergence plot over time for the ELE and VDW legs of the Ligand 8 complex phase using Lambda-ABF and Lambda-ABF-OPES method

in a single replica. In this case, the acceleration in convergence time is a factor of 9 for ELE and 4 for VDW. When considering different replicas, the convergence speedup for ELE ranges from 5 to 9 times, while for VDW, it ranges from 3 to 5 times.

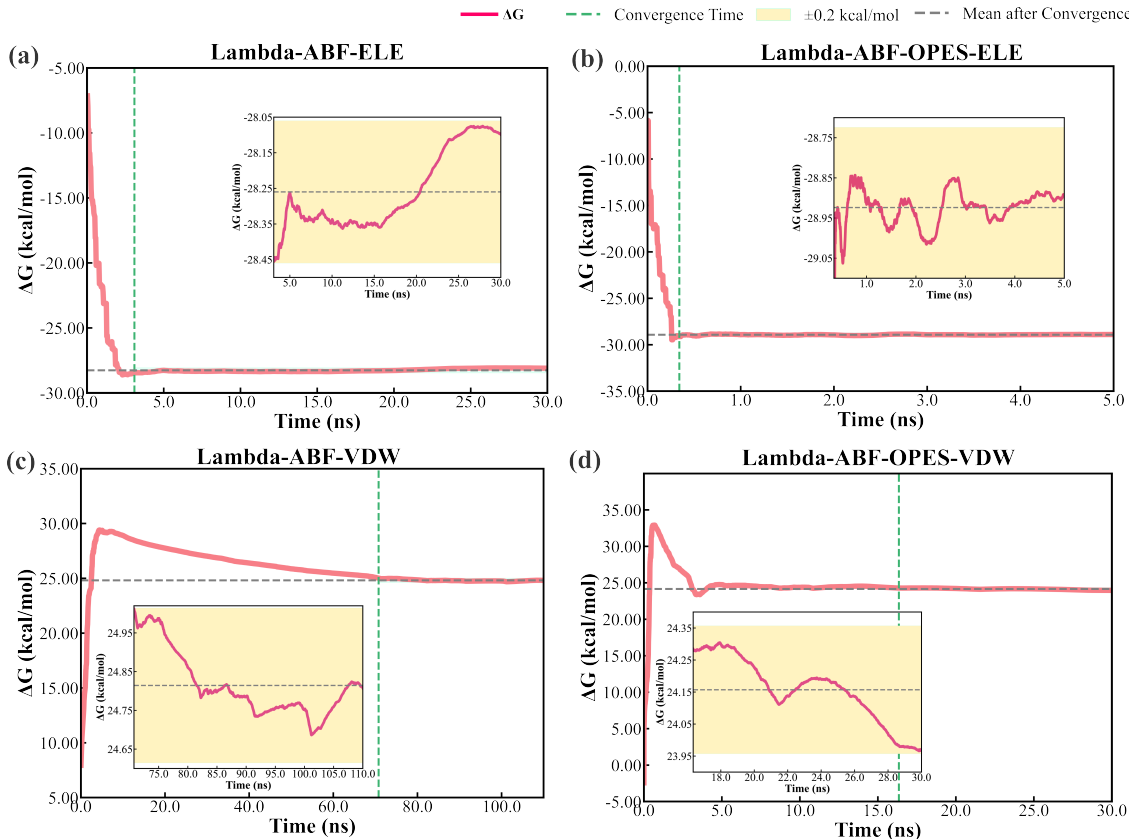


Figure 4: ΔG convergence comparison between Lambda-ABF and Lambda-ABF-OPES. The ΔG over time for the (a)-(b) ELE leg and the (c)-(d) VDW leg of Ligand 8, calculated using Lambda-ABF and Lambda-ABF-OPES methods, respectively. Each panel includes a zoomed-in plot of the converged area.

The convergence analysis results for all ligands using Lambda-ABF-OPES are summarized in Table 1. The average convergence time for the complex phase was less than 3 ns for the ELE leg and approximately 20 ns for the VDW leg, highlighting the rapid stabilization of the ΔG in these components. In the solvent phase, the ELE leg showed convergence for most ligands within 1–2 ns or less, while the VDW leg converged within 2–3 ns. These results demonstrate a marked improvement in convergence speed compared to other currently used methods, which typically requires significantly longer simulation times to achieve comparable

stability³⁹⁻⁴¹

In practical applications, such efficiency gains can translate into a substantial reduction in computational costs, enabling more extensive exploration of chemical space or greater statistical sampling within the same resource constraints. The combination of simplicity, accuracy, and computational efficiency makes this approach a promising tool for the drug discovery field.

Table 1: Summary of the BRD4 binding free energy results using Lambda-ABF-OPES. The experimental (ΔG_{exp}) and calculated (ΔG_{calc}) values for each ligand are presented. All ΔG values are reported in kcal/mol. The calculated ΔG_{calc} and associated errors represent the mean and standard error of the mean, derived from three replicates for each ligand. The PDB files used as input are listed. The average convergence time over three replicas for each ELE and VDW leg in the complex and solvent phases is reported in ns per replica. The total simulation time for the ELE and VDW legs in the complex phase is 5 ns and 30 ns per walker, respectively. For the solvent phase, each leg is run for 5 ns per walker.

Compound	ΔG_{exp}	ΔG_{calc}	$\Delta G_{\text{calc}} - \Delta G_{\text{exp}}$	PDB	ns per walker			
					Complex		Solvent	
					ELE	VDW	ELE	VDW
L1	-9.8 ± 0.1 ⁶¹	-10.56 ± 0.46	-0.85	4OGI	0.9	22.5	1.9	3.5
L2	-9.6 ± 0.1 ⁶²	-8.26 ± 0.22	1.34	3MXF	2.2	19.2	0.9	2.2
L3	-9.0 ± 0.1 ⁶³	-9.19 ± 0.30	-0.19	4MR3	2.6	17.8	0.4	2.4
L4	-8.9 ± 0.1 ⁶¹	-10.13 ± 0.15	-1.23	4OGJ	2.6	24.8	2.7	3.5
L5	-8.8 ± 0.1 ⁶⁴	-8.27 ± 0.52	0.09	4J0R	2.1	15.9	0.9	2.7
L6	-8.2 ± 0.1 ⁶⁵	-6.75 ± 0.30	1.45	3U5L	0.6	20.2	0.5	3.5
L7	-7.8 ± 0.1 ⁶³	-6.42 ± 0.65	1.38	4MR4	0.9	20.0	1.4	3.4
L8	-7.4 ± 0.1 ⁶⁵	-5.46 ± 0.53	1.94	3U5J	0.7	20.7	0.4	2.5
L9	-7.3 ± 0.1 ⁶⁴	-7.57 ± 0.12	-0.27	3SVG	1.5	17.4	0.5	2.7
L10	-6.3 ± 0.0 ⁶⁶	-7.05 ± 0.33	-0.75	4HBV	1.8	14.8	0.2	1.6
L11	-5.6 ⁶⁷	-4.98 ± 0.58	0.62	Model	0.2	10.7	0.2	1.9

Conclusions

Accurately predicting the binding affinity between small molecules and their target proteins remains a critical challenge in drug discovery, with far-reaching implications for the speed and efficiency of therapeutic development.

In this study, we introduced a new hybrid approach that combines Lambda-ABF with the exploratory version of the OPES method. This novel integration leverages the complementary strengths of ABF and OPES to overcome critical limitations in alchemical free energy

calculations, including inefficient exploration of configurational space and kinetic trapping in energy landscapes. By applying biases to the Lambda collective variable (CV) and incorporating the AMOEBA polarizable force field alongside DBC restraints, our method achieves unprecedented levels of sampling efficiency, up to nine times faster than the original Lambda-ABF technique.

Our application of this hybrid method to a diverse set of 11 drug-like molecules targeting BRD4 bromodomains yielded close alignment between our computational results and experimental data with a mean absolute error of 0.9 kcal/mol. Importantly, this was achieved while using the highly accurate AMOEBA polarizable force field, demonstrating the feasibility of this approach for real-world drug discovery applications. This approach can be naturally extended to neural networks methodologies including Machine Learning Interatomic Potentials (MLIP)^{68,69} and Foundation models whose additional computational cost for free energy computations compared to FFs has limited to date their use in production.

By integrating state-of-the-art methodologies and harnessing their synergistic advantages, this work provides a robust tool for the rapid and reliable advancement of novel therapeutics. Though applied in an alchemical context in this study, this methodology shows promise for broader applicability within enhanced sampling techniques and lays the groundwork for its integration into a more general framework, which we plan to further investigate in future work.

Conflict of interest/Competing interests

L. L., and J.-P. P. are co-founders and shareholders of Qubit Pharmaceuticals. The remaining authors declare no competing interests.

Acknowledgment

We thank Haochuan Chen for implementing OPES in the Colvars library, building on Michele Invernizzi's work. We also thank Chengwen Liu and Timothé Melin (Qubit Pharmaceuticals) for their assistance with the parameterization of complex ligands. We thank the Grand Équipement de Calcul Intensif (GENCI), Institut du Développement et des Ressources en Informatique (IDRIS), and Centre Informatique de l'Enseignement Supérieur (CINES), France, for their support of this work through grant no. AD010715770 and A0160714153. This work has received funding from the European Research Council (ERC) under the European Union's Horizon 2020 research and innovation program (grant agreement No 810367), project EMC2 (JPP).

Technical Appendix

Analytical lambda derivatives for the polarization energy using Particle Mesh Ewald

A simple interpolation of polarization between the end states reads:

$$E_{pol}(\mathbf{r}, \lambda) = \lambda E_{pol}(\mathbf{r}, 1) + (1 - \lambda) E_{pol}(\mathbf{r}, 0)$$

so that:

$$\frac{\partial E_{pol}}{\partial \lambda}(\mathbf{r}, \lambda) = E_{pol}(\mathbf{r}, 1) - E_{pol}(\mathbf{r}, 0)$$

which requires two resolutions of the polarization equations per timestep as stated in the main text. Alternatively, let's consider the polarization energy associated to a scaling of the polarizabilities and the permanent multipoles of the "alchemical" part of the system, the

complete system being made of N atoms:

$$E_{pol}(\mathbf{r}, \lambda, \boldsymbol{\mu}(\mathbf{r}, \lambda)) = \frac{1}{2} \boldsymbol{\mu} \mathbf{T}(\mathbf{r}, \lambda) \boldsymbol{\mu} - \boldsymbol{\mu} \mathbf{E}(\mathbf{r}, \lambda)$$

where \mathbf{T} is the (3N,3N) polarization matrix and \mathbf{E} the 3N vector of the permanent electric fields on the polarizable sites. The Hellman-Feynman theorem yields:

$$\frac{dE_{pol}}{d\lambda} = \frac{1}{2} \boldsymbol{\mu} \frac{\partial \mathbf{T}}{\partial \lambda} \boldsymbol{\mu} - \boldsymbol{\mu} \frac{\partial \mathbf{E}}{\partial \lambda}$$

The derivative contribution due to the \mathbf{T} is trivial to compute because it is only associated to its diagonal part $\boldsymbol{\alpha}^{-1}(\lambda)$, with $\boldsymbol{\alpha}$ collecting the diagonal polarizability tensors. In the context of periodic boundary conditions computed with Particle Mesh Ewald, the second one can be separated in 3 given the various component of $\frac{\partial \mathbf{E}}{\partial \lambda} = \frac{\partial \mathbf{E}_{real}}{\partial \lambda} + \frac{\partial \mathbf{E}_{self}}{\partial \lambda} + \frac{\partial \mathbf{E}_{recip}}{\lambda}$. The first two terms can be directly computed. If only fixed charge are used (and no permanent multipoles) then the last one can be reformulated as:

$$\frac{\partial}{\partial \lambda} (\boldsymbol{\mu} \mathbf{E}_{recip}(\lambda)) = \frac{\partial}{\partial \lambda} (\mathbf{Q}(\lambda) \mathbf{V}_{recip}(\boldsymbol{\mu})) = \frac{\partial}{\partial \lambda} (\mathbf{Q}(\lambda)) \mathbf{V}_{recip}(\boldsymbol{\mu})$$

where $\mathbf{Q}(\lambda)$ is the vector (of size N) containing the permanent charges and \mathbf{V}_{recip} the vector of same size containing the reciprocal potential due to the induced dipoles. This potential is readily available to compute the permanent polarization energy and $\frac{\partial \mathbf{Q}(\lambda)}{\partial \lambda}$ is trivial to compute. The same reasoning is naturally extended to permanent multipoles of higher order by involving derivatives of $V_{recip}(\boldsymbol{\mu})$ which are always available to compute the permanent polarization energy.

References

- (1) de Azevedo, J.; Walter, F.; Dias, R. Computational methods for calculation of ligand-binding affinity. Curr. Drug Targets. **2008**, 9, 1031–1039.
- (2) Schindler, C. E. M. et al. Large-Scale assessment of binding free energy calculations in active drug discovery projects. J. Chem. Inf. Model. **2020**, 60, 5457–5474, PMID: 32813975.
- (3) Bernardi, R. C.; Melo, M. C.; Schulten, K. Enhanced sampling techniques in molecular dynamics simulations of biological systems. Biochimica et Biophysica Acta (BBA)-General Subjects **2015**, 1850, 872–877.
- (4) Hénin, J.; Lelièvre, T.; Shirts, M. R.; Valsson, O.; Delemotte, L. Enhanced Sampling Methods for Molecular Dynamics Simulations [Article v1.0]. Living J. Comput. Mol. Sci. **2022**, 4, 1583.
- (5) Mehdi, S.; Smith, Z.; Herron, L.; Zou, Z.; Tiwary, P. Enhanced sampling with machine learning. Annu. Rev. Phys. Chem. **2024**, 75.
- (6) Gresh, N.; Cisneros, G. A.; Darden, T. A.; Piquemal, J.-P. Anisotropic, polarizable molecular mechanics studies of inter-and intramolecular interactions and ligand- macro-molecule complexes. A bottom-up strategy. J. Chem. Theory Comput. **2007**, 3, 1960–1986.
- (7) Shi, Y.; Ren, P.; Schnieders, M.; Piquemal, J.-P. Reviews in Computational Chemistry; Polarizable Force Fields for Biomolecular Modeling, John Wiley and Sons, Ltd, 2015; Vol. 28; Chapter 2, pp 51–86.
- (8) Melcr, J.; Piquemal, J.-P. Accurate biomolecular simulations account for electronic polarization. Front. Mol. Biosci. **2019**, 6, 143.

- (9) Ponder, J. W.; Wu, C.; Ren, P.; Pande, V. S.; Chodera, J. D.; Schnieders, M. J.; Haque, I.; Mobley, D. L.; Lambrecht, D. S.; DiStasio Jr, R. A., et al. Current status of the AMOEBA polarizable force field. *J. Phys. Chem. B* **2010**, *114*, 2549–2564.
- (10) Wu, J. C.; Chattree, G.; Ren, P. Automation of AMOEBA polarizable force field parameterization for small molecules. *Theor. Chem. Acc.* **2012**, *131*, 1–11.
- (11) Shi, Y.; Xia, Z.; Zhang, J.; Best, R.; Wu, C.; Ponder, J. W.; Ren, P. Polarizable atomic multipole-based AMOEBA force field for proteins. *J. Chem. Theory Comput.* **2013**, *9*, 4046–4063.
- (12) Zhang, C.; Lu, C.; Jing, Z.; Wu, C.; Piquemal, J.-P.; Ponder, J. W.; Ren, P. AMOEBA polarizable atomic multipole force field for nucleic acids. *J. Chem. Theory Comput.* **2018**, *14*, 2084–2108, PMID: 29438622.
- (13) Walker, B.; Liu, C.; Wait, E.; Ren, P. Automation of AMOEBA polarizable force field for small molecules: Poltype 2. *J. Comput. Chem.* **2022**, *43*, 1530–1542.
- (14) Laury, M. L.; Wang, Z.; Gordon, A. S.; Ponder, J. W. Absolute binding free energies for the SAMPL6 cucurbit [8] uril host–guest challenge via the AMOEBA polarizable force field. *J. Comput.-Aided Mol. Des.* **2018**, *32*, 1087–1095.
- (15) Inizan, T. J.; Célerse, F.; Adjoua, O.; El Ahdab, D.; Jolly, L.-H.; Liu, C.; Ren, P.; Montes, M.; Lagarde, N.; Lagardère, L., et al. High-resolution mining of the SARS-CoV-2 main protease conformational space: supercomputer-driven unsupervised adaptive sampling. *Chem. Sci.* **2021**, *12*, 4889–4907.
- (16) El Khoury, L. et al. Computationally driven discovery of SARS-CoV-2 Mpro inhibitors: from design to experimental validation. *Chem. Sci.* **2022**, *13*, 3674–3687.
- (17) Chung, M. K.; Miller, R. J.; Novak, B.; Wang, Z.; Ponder, J. W. Accurate host–guest

- binding free energies using the AMOEBA polarizable force field. J. Chem. Inf. Model. **2023**, 63, 2769–2782.
- (18) Blazhynska, M.; Lagardère, L.; Liu, C.; Adjoua, O.; Ren, P.; Piquemal, J.-P. Water–glycan interactions drive the SARS-CoV-2 spike dynamics: insights into glycan-gate control and camouflage mechanisms. Chem. Sci. **2024**, 15, 14177–14187.
- (19) Ansari, N.; Liu, C.; Hedin, F.; Hénin, J.; Ponder, J.; Ren, P.; Piquemal, J.-P.; Lagardère, L.; El Hage, K. Targeting RNA with small molecules using state-of-the-art methods provides highly predictive affinities of Riboswitch inhibitors. **2024**,
- (20) Torrie, G. M.; Valleau, J. P. Nonphysical sampling distributions in Monte Carlo free-energy estimation: Umbrella sampling. J. Comput. Phys. **1977**, 23, 187–199.
- (21) Darve, E.; Pohorille, A. Calculating free energies using average force. J. Chem. Phys. **2001**, 115, 9169–9183.
- (22) Darve, E.; Rodríguez-Gómez, D.; Pohorille, A. Adaptive biasing force method for scalar and vector free energy calculations. J. Chem. Phys. **2008**, 128.
- (23) Comer, J.; Gumbart, J. C.; Hénin, J.; Lelièvre, T.; Pohorille, A.; Chipot, C. The adaptive biasing force method: Everything you always wanted to know but were afraid to ask. J. Phys. Chem. B **2015**, 119, 1129–1151.
- (24) Laio, A.; Parrinello, M. Escaping free-energy minima. Proc. Natl. Acad. Sci. **2002**, 99, 12562–12566.
- (25) Barducci, A.; Bonomi, M.; Parrinello, M. Metadynamics. Wiley Interdiscip. Rev. Comput. Mol. Sci. **2011**, 1, 826–843.
- (26) Invernizzi, M.; Parrinello, M. Rethinking Metadynamics: From bias potentials to probability Distributions. J. Phys. Chem. Lett. **2020**, 11, 2731–2736.

- (27) Invernizzi, M.; Parrinello, M. Exploration vs convergence speed in adaptive-bias enhanced sampling. J. Chem. Theory Comput. **2022**, 18, 3988–3996.
- (28) Maragliano, L.; Vanden-Eijnden, E. A temperature accelerated method for sampling free energy and determining reaction pathways in rare events simulations. Chem. Phys. Lett. **2006**, 426, 168–175.
- (29) Fu, H.; Shao, X.; Cai, W.; Chipot, C. Taming rugged free energy landscapes using an average force. Acc. Chem. Res. **2019**, 52, 3254–3264.
- (30) Williams-Noonan, B. J.; Yuriev, E.; Chalmers, D. K. Free energy methods in drug design: prospects of “alchemical perturbation” in medicinal chemistry: miniperspective. J. Med. Chem. **2018**, 61, 638–649.
- (31) Zwanzig, R. W. High-temperature equation of state by a perturbation method. I. Non-polar gases. J. Chem. Phys. **1954**, 22, 1420–1426.
- (32) Straatsma, T.; McCammon, J. Multiconfiguration thermodynamic integration. J. Chem. Phys. **1991**, 95, 1175–1188.
- (33) Kong, X.; Brooks, C. L. λ -dynamics: A new approach to free energy calculations. J. Chem. Phys. **1996**, 105, 2414–2423.
- (34) Lagardère, L.; Maurin, L.; Adjoua, O.; El Hage, K.; Monmarché, P.; Piquemal, J.-P.; Hémin, J. Lambda-ABF: Simplified, portable, accurate, and cost-effective alchemical free-energy computation. J. Chem. Theory Comput. **2024**, 20, 4481–4498, PMID: 38805379.
- (35) Minoukadeh, K.; Chipot, C.; Lelièvre, T. Potential of mean force calculations: a multiple-walker adaptive biasing force approach. J. Chem. Theory Comput. **2010**, 6, 1008–1017.

- (36) Salari, R.; Joseph, T.; Lohia, R.; Hénin, J.; Brannigan, G. A Streamlined, general approach for computing ligand binding free energies and its application to GPCR-bound cholesterol. J. Chem. Theory Comput. **2018**, 14, 6560–6573, PMID: 30358394.
- (37) Fiorin, G.; Klein, M. L.; Hénin, J. Using collective variables to drive molecular dynamics simulations. Mol. Phys. **2013**, 111, 3345–3362.
- (38) Fiorin, G.; Marinelli, F.; Forrest, L. R.; Chen, H.; Chipot, C.; Kohlmeyer, A.; Santuz, H.; Hénin, J. Expanded functionality and portability for the Colvars library. J. Phys. Chem. B **2024**, 128, 11108–11123.
- (39) Gapsys, V.; Yildirim, A.; Aldeghi, M.; Khalak, Y.; Van der Spoel, D.; de Groot, B. L. Accurate absolute free energies for ligand–protein binding based on non-equilibrium approaches. Commun. Chem. **2021**, 4, 61.
- (40) Karrenbrock, M.; Borsatto, A.; Rizzi, V.; Lukauskis, D.; Aureli, S.; Luigi Gervasio, F. Absolute binding free energies with OneOPES. J. Phys. Chem. Lett. **2024**, 15, 9871–9880.
- (41) Aldeghi, M.; Heifetz, A.; Bodkin, M. J.; Knapp, S.; Biggin, P. C. Accurate calculation of the absolute free energy of binding for drug molecules. Chem. Sci. **2016**, 7, 207–218.
- (42) Bhati, A. P.; Wan, S.; Coveney, P. V. Equilibrium and nonequilibrium ensemble methods for accurate, precise and reproducible absolute binding free energy calculations. J. Chem. Theory Comput. **2024**,
- (43) Lagardère, L.; Jolly, L.-H.; Lipparini, F.; Aviat, F.; Stamm, B.; Jing, Z. F.; Harger, M.; Torabifard, H.; Cisneros, G. A.; Schnieders, M. J., et al. Tinker-HP: a massively parallel molecular dynamics package for multiscale simulations of large complex systems with advanced point dipole polarizable force fields. Chem. Sci. **2018**, 9, 956–972.

- (44) Adjoua, O.; Lagardère, L.; Jolly, L.-H.; Durocher, A.; Very, T.; Dupays, I.; Wang, Z.; Inizan, T. J.; Célerse, F.; Ren, P., et al. Tinker-HP: Accelerating molecular dynamics simulations of large complex systems with advanced point dipole polarizable force fields using GPUs and multi-GPU systems. *J. Chem. Theory Comput.* **2021**, *17*, 2034–2053.
- (45) Lagardère, L.; Aviat, F.; Piquemal, J.-P. Pushing the limits of multiple-time-step strategies for polarizable point dipole molecular dynamics. *J. Phys. Chem. Lett.* **2019**, *10*, 2593–2599.
- (46) Bussi, G.; Donadio, D.; Parrinello, M. Canonical sampling through velocity rescaling. *J. Chem. Phys.* **2007**, *126*.
- (47) Berendsen, H. J.; Postma, J. v.; Van Gunsteren, W. F.; DiNola, A.; Haak, J. R. Molecular dynamics with coupling to an external bath. *J. Chem. Phys.* **1984**, *81*, 3684–3690.
- (48) Essmann, U.; Perera, L.; Berkowitz, M. L.; Darden, T.; Lee, H.; Pedersen, L. G. A smooth particle mesh Ewald method. *J. Chem. Phys.* **1995**, *103*, 8577–8593.
- (49) Lagardère, L.; Lipparini, F.; Polack, E.; Stamm, B.; Cancès, E.; Schnieders, M.; Ren, P.; Maday, Y.; Piquemal, J.-P. Scalable evaluation of polarization energy and associated forces in polarizable molecular dynamics: II. Toward massively parallel computations using smooth particle mesh Ewald. *J. Chem. Theory Comput.* **2015**, *11*, 2589–2599.
- (50) Kirkwood, J. G. Statistical mechanics of fluid mixtures. *J. Chem. Phys.* **1935**, *3*, 300–313.
- (51) Santiago-McRae, E.; Ebrahimi, M.; Sandberg, J. W.; Brannigan, G.; Hénin, J. Computing absolute binding affinities by streamlined alchemical free energy perturbation (safep)[article v1. 0]. *Living J. Comput. Mol. Sci.* **2023**, *5*, 2067–2067.
- (52) Lelièvre, T.; Rousset, M.; Stoltz, G. Computation of free energy profiles with parallel adaptive dynamics. *J. Chem. Phys.* **2007**, *126*.

- (53) Beutler, T. C.; Mark, A. E.; van Schaik, R. C.; Gerber, P. R.; Van Gunsteren, W. F. Avoiding singularities and numerical instabilities in free energy calculations based on molecular simulations. Chem. Phys. Lett. **1994**, 222, 529–539.
- (54) Kaus, J. W.; Harder, E.; Lin, T.; Abel, R.; McCammon, J. A.; Wang, L. How to deal with multiple binding poses in alchemical relative protein–ligand binding free energy calculations. J. Chem. Theory Comput. **2015**, 11, 2670–2679.
- (55) Thiel, A. C.; Speranza, M. J.; Jadhav, S.; Stevens, L. L.; Unruh, D. K.; Ren, P.; Ponder, J. W.; Shen, J.; Schnieders, M. J. Constant-pH simulations with the polarizable atomic multipole AMOEBA force field. J. Chem. Theory Comput. **2024**, 20, 2921–2933.
- (56) Lipparini, F.; Barone, V. Polarizable force fields and polarizable continuum model: A fluctuating charges/PCM approach. 1. Theory and implementation. J. Chem. Theory Comput. **2011**, 7, 3711–3724.
- (57) Lipparini, F.; Lagardère, L.; Raynaud, C.; Stamm, B.; Cancès, E.; Mennucci, B.; Schnieders, M.; Ren, P.; Maday, Y.; Piquemal, J.-P. Polarizable Molecular Dynamics in a Polarizable Continuum Solvent. J. Chem. Theory Comput. **2015**, 11, 623–634.
- (58) Loco, D.; Polack, É.; Caprasecca, S.; Lagardère, L.; Lipparini, F.; Piquemal, J.-P.; Mennucci, B. A QM/MM approach using the AMOEBA polarizable embedding: from ground state energies to electronic excitations. J. Chem. Theory Comput. **2016**, 12, 3654–3661.
- (59) Loco, D.; Lagardère, L.; Adjoua, O.; Piquemal, J.-P. Atomistic polarizable embeddings: energy, dynamics, spectroscopy, and reactivity. Acc. Chem. Res. **2021**, 54, 2812–2822, PMID: 33961401.
- (60) Aldeghi, M.; Ross, G. A.; Bodkin, M. J.; Essex, J. W.; Knapp, S.; Biggin, P. C. Large-scale analysis of water stability in bromodomain binding pockets with grand canonical Monte Carlo. Commun. Chem. **2018**, 1, 19.

- (61) Ciceri, P.; Müller, S.; O'mahony, A.; Fedorov, O.; Filippakopoulos, P.; Hunt, J. P.; Lasater, E. A.; Pallares, G.; Picaud, S.; Wells, C., et al. Dual kinase-bromodomain inhibitors for rationally designed polypharmacology. Nat. Chem. Biol. **2014**, 10, 305–312.
- (62) Filippakopoulos, P.; Qi, J.; Picaud, S.; Shen, Y.; Smith, W. B.; Fedorov, O.; Morse, E. M.; Keates, T.; Hickman, T. T.; Felletar, I., et al. Selective inhibition of BET bromodomains. Nature **2010**, 468, 1067–1073.
- (63) Picaud, S.; Wells, C.; Felletar, I.; Brotherton, D.; Martin, S.; Savitsky, P.; Diez-Dacal, B.; Philpott, M.; Bountra, C.; Lingard, H., et al. RVX-208, an inhibitor of BET transcriptional regulators with selectivity for the second bromodomain. Proc. Natl. Acad. Sci. **2013**, 110, 19754–19759.
- (64) Hewings, D. S.; Fedorov, O.; Filippakopoulos, P.; Martin, S.; Picaud, S.; Tumber, A.; Wells, C.; Olcina, M. M.; Freeman, K.; Gill, A., et al. Optimization of 3, 5-dimethylisoxazole derivatives as potent bromodomain ligands. J. Med. Chem. **2013**, 56, 3217–3227.
- (65) Filippakopoulos, P.; Picaud, S.; Fedorov, O.; Keller, M.; Wrobel, M.; Morgenstern, O.; Bracher, F.; Knapp, S. Benzodiazepines and benzotriazepines as protein interaction inhibitors targeting bromodomains of the BET family. Bioorg. Med. Chem. **2012**, 20, 1878–1886.
- (66) Fish, P. V.; Filippakopoulos, P.; Bish, G.; Brennan, P. E.; Bunnage, M. E.; Cook, A. S.; Fedorov, O.; Gerstenberger, B. S.; Jones, H.; Knapp, S., et al. Identification of a chemical probe for bromo and extra C-terminal bromodomain inhibition through optimization of a fragment-derived hit. J. Med. Chem. **2012**, 55, 9831–9837.
- (67) Vidler, L. R.; Filippakopoulos, P.; Fedorov, O.; Picaud, S.; Martin, S.; Tomsett, M.; Woodward, H.; Brown, N.; Knapp, S.; Hoelder, S. Discovery of novel small-molecule

- inhibitors of BRD4 using structure-based virtual screening. J. Med. Chem. **2013**, 56, 8073–8088.
- (68) Plé, T.; Lagardère, L.; Piquemal, J.-P. Force-field-enhanced neural network interactions: from local equivariant embedding to atom-in-molecule properties and long-range effects. Chem. Sci. **2023**, 14, 12554–12569.
- (69) Plé, T.; Adjoua, O.; Lagardère, L.; Piquemal, J.-P. FeNNol: An efficient and flexible library for building force-field-enhanced neural network potentials. J. Chem. Phys. **2024**, 161, 042502.